

## Time-resolved fluorescent X-ray interference

Y. C. Sasaki,<sup>a\*</sup> Y. Suzuki,<sup>b</sup> H. Yamanashi,<sup>c</sup> A. Arai<sup>d</sup> and M. Yanagihara<sup>d</sup>

<sup>a</sup>Advanced Research Laboratory, Hitachi Ltd, Hatoyama, Saitama, Japan, <sup>b</sup>Japan Synchrotron Radiation Research Institute (JASRI), SPring-8, Kamigori, Hyogo, Japan, <sup>c</sup>Central Research Laboratory, Hitachi Ltd, Higashi-koigakubo, Kokubunji-shi, Japan, and <sup>d</sup>Research Institute for Scientific Measurements, Tohoku University, 2-1-1 Katahira, Aoba-ku, Sendai, Japan. E-mail: ycsasaki@harl.hitachi.co.jp

(Received 4 August 1997; accepted 13 February 1998)

A fluorescent X-ray interference method can effectively measure nanometer-level conformational changes for non-crystallized molecules and proteins in aqueous conditions. The time-resolved technique can be used to obtain information about the dynamics of molecules and proteins. Instrumentation for time-resolved fluorescent X-ray interference has been designed. A typical interference-fringe pattern was observed with approximately 3 s of X-ray exposure time from K-fluorescent X-rays emitted from a Zn monoatomic layer on an Rh substrate. The primary X-ray beam was polychromed with a mirror for total external reflection of X-rays and was tuned to an energy level at which only Zn K radiation became optimally excited. The glancing angle of the primary X-ray beam was fixed at a glancing angle at which the total intensity of K-fluorescent X-rays emitted from Zn atoms corresponded to the maximum value. The fluorescent X-ray interference fringes were monitored with an imaging plate (IP) as a non-energy-dispersive two-dimensional detector. The exposed interference fringes on the IP were integrated along the direction of the fringes. The integrated fringes were in close agreement with a theoretical estimate based on the interference among transmitted and reflected waves at interfaces in the sample.

**Keywords:** time-resolved technique; fluorescent X-ray interference; polychromatic primary beam; imaging plates.

### 1. Introduction

Time-resolved observations of conformational changes in functional protein molecules and membranes are important to the understanding of biological phenomena. The functional activities of biomolecules are maintained under limited aqueous environments. The fluorescent X-ray interference (FXI) method can effectively measure nanometer-level structural information about non-crystallized proteins in the appropriate aqueous conditions (Sasaki *et al.*, 1994). Information obtained from our FXI method is similar to that from X-ray standing waves (XSW). In a conventional XSW technique, essentially monochromatic X-rays are used as a primary probe (Bedzyk *et al.*, 1989). Polychromatic X-rays derived from synchrotron radiation can be used in FXI experiments because fluorescent X-ray radiation occurs independently of the primary X-ray beam. Although the incident angle of the primary X-ray beam is a parameter in the XSW

technique, the glancing angle for the primary beam is fixed during the X-ray exposure time in FXI experiments. The pattern of the observed fluorescent X-ray interference fringes can be obtained without scanning the incident angles.

In addition, the intensity of the observed two-dimensional fluorescent X-ray patterns can be integrated along the fringe direction because the observed fluorescent X-rays show patterns similar to those of Young's fringes (Sasaki *et al.*, 1993). The designed time-resolved FXI technique thus offers advantages for the recording of fluorescent X-ray interference fringes from a short-lived bimolecular complex during biochemical reactions.

### 2. Theory

We used the Lloyd's mirror-type interference effect on monochromatic X-rays from fluorescent X-ray emitting atoms embedded in a non-crystalline material, as shown in Fig. 1 (Born & Wolf, 1980). X-ray emissions from atoms located above a substrate surface can take two optical paths: direct emission and totally reflected emission when the take-off angle ( $\theta_i$ ) is smaller than the critical angle ( $\theta_c$ ) for total external reflection of the observed fluorescent X-rays. The coherent sources are the primary source  $S_1$ , which is the fluorescent X-ray atom above the substrate surface, and its virtual image  $S_2$ , as shown in Fig. 1. The optical path difference,  $\Delta$ , between the two sources depends on the distance ( $z$ ) of the fluorescent X-ray emitting atom from the substrate and the phase shift that occurs with X-ray total external reflection on the substrate surface. The geometrical path difference is described as  $\Delta = 2z \sin \theta_i$ . Thus, positional information on the emitting atoms can be obtained from the period of the observed interference fringes.

This interference of fluorescent X-rays is considered to be a time-inverse phenomenon of XSW experiments, and can also be regarded as a special case of X-ray holographic microscopy using a local reference beam. This three-dimensional local-beam holography is considered to be a powerful technique for determining the atomic scale position of neighbouring atoms (Tegze & Faigel, 1996). The FXI technique can be applied to the analysis of one-dimensional nanometer-level structures. If the arrangement of adsorbed biomolecules is controlled on the substrate surface, we can obtain three-dimensional information about the adsorbed biomolecules from the FXI experiments.

The theoretical interference pattern from X-ray emissions can be calculated for a characteristic matrix of stratified media on the basis of reciprocity. In other words, the calculation of the char-

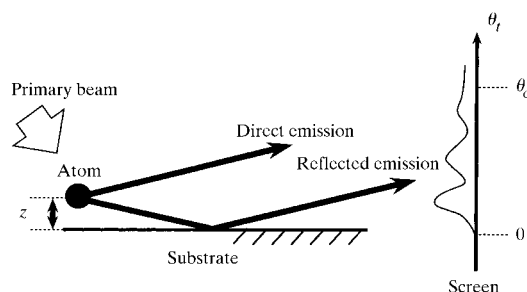


**Figure 1** Schematic diagram of the interference phenomenon of fluorescent X-rays from an emitting atom embedded within a sample.  $z$  represents the distance between the radioactive atom and the substrate surface.  $\theta_i$  is the take-off angle of the fluorescent X-rays. The model interference fringes under  $\theta_c$  are shown on the screen.

acteristic X-ray intensity from coordinate  $z$  for take-off angle  $\theta_i$  is identical to that of the incident X-ray field at coordinate  $z$  for glancing angle  $\theta_r$ . Although X-ray emissions from atoms have a spherical waveform, a plane wave was observed under the conditions maintained for this experiment. This is because the distance between the observation point and the atomic source points is very long. Thus, the observed wave can be regarded as a plane wave which is a component of a spherical wave.

When radioactive atoms act as characteristic X-ray sources with distribution  $N$ , the yield  $Y$  is given by

$$I(\theta_i, z) = |E_d + E_r|^2, \quad (1)$$

$$Y(\theta_i) = \int N(z) I(\theta_i, z) dz, \quad (2)$$

where  $I(\theta_i, z)$  is the intensity of the characteristic X-rays resulting from the interference effects between the direct and totally reflected emissions from coordinate  $z$  at the take-off angle,  $\theta_i$ .  $E_d$  and  $E_r$  are  $E$ -field plane waves for the direct and reflected emissions, and  $N(z)$  is the atom distribution at distance  $z$  from the substrate surface.

### 3. Experiment

The experimental set-up is shown in Fig. 2. This experiment was carried out at the BL-8C2 experimental station on the KEK Photon Factory 2.5 GeV storage ring (Hirai *et al.*, 1993). The stored current was between 300 and 350 mA. Synchrotron radiation was used for the polychromatic X-ray source. The mirror for the X-ray total external reflection was quartz substrate and the filter used was made of aluminium foil. The primary polychromatic X-ray beam was tuned to an energy level at which the observed fluorescent X-rays became optimally excited. The beam was reflected at the glancing angle at which the total intensity of the fluorescent X-ray was maximized. The exposed area for the sample was  $5 \times 35$  mm. The output beam from the synchrotron radiation was monitored by using an ionization chamber. The incident X-ray beam of the sample was narrowed to  $100 \mu\text{m}$  (V)  $\times$   $5$  mm (H) by slits. Incident radiation was linearly polarized, and the electrical vector was in the horizontal plane. Fluorescent radiation was measured at a  $90^\circ$  scattering angle in the horizontal plane to minimize background signals caused by elastic scattering.

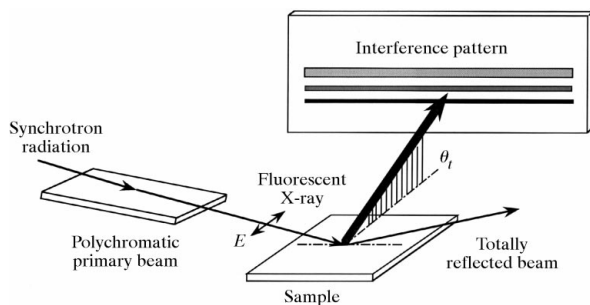


**Figure 2**

Schematic drawing of the experimental apparatus for the time-resolved FXI technique. Synchrotron radiation was used for the polychromatic X-ray beam, with a mirror for X-ray total external reflection. The glancing angle for the primary X-ray beam is fixed at an angle at which the total intensity of fluorescent X-rays was maximized. We used an imaging plate as a two-dimensional detector to observe the overall structure of the interference fringes.

In this experiment, the FXI fringes were monitored with a non-energy-dispersive two-dimensional detector (IP, BAS-5000, Fuji Film Co.; a wide-area detector) and by scanning the slit with an energy-dispersive detector (a pure-Ge detector). The time-resolved FXI technique needs a two-dimensional detector to observe the overall structure of the interference fringes and to integrate the intensity of the fluorescent X-rays along the direction of the fringes. In addition, we use polychromatic X-rays derived from synchrotron radiation to increase the intensity of the observed fluorescent X-rays in this experiment. In general, fluorescent X-rays excited using polychromatic X-rays emit twin fluorescent X-rays, for example,  $K\alpha$  and  $K\beta$  radiation or  $L\alpha$  and  $L\beta$  radiation. The monitored FXI pattern will thus be from a mixture of these radiations when we use an IP which is a non-energy-dispersive two-dimensional detector. The dimensions of the IP are  $20 \times 25$  mm, and the pixel size of the IP is  $25 \mu\text{m}$ . A flat cassette with a sample-to-IP distance of 300 mm can be mounted on the camera. The IP cassette was driven horizontally directly by the stepping motor, whose position was monitored by a linear sensor. The maximum speed of the stepping motor is  $40 \text{ mm s}^{-1}$ . The IP was read out by a BAS-5000 system (Fuji Film Co.). The IP camera was designed to have the slit [ $5 \text{ mm}$  (V)  $\times$   $20 \text{ mm}$  (H)] restricting the exposure area of the IP and to allow the vertical translation of the IP cassette for continuous measurement. The IP cassette is covered with a 6 mm-thick Pb shield box to suppress background signals. The intensity of the IP between  $-3$  and  $0$  mrad take-off angle was defined as the background level necessary for subtracting the background radiation. The linearity of the IP was confirmed for  $\text{Cu } K\beta$  and  $\text{Mo } K\alpha$  (Miyahara *et al.*, 1986).

The IP has no energy selectivity. Thus, a Ge detector was used as a fluorescent X-ray detector to compare the experimental results with the theoretical ones. A  $20 \mu\text{m}$  (V)  $\times$   $12 \text{ mm}$  (H) slit was used to determine the take-off angle for the fluorescent X-rays and was placed in front of the detector at a distance of 90 mm from the sample. The angular distribution of the fluorescent X-rays was measured by scanning the slit along the transversal direction. This arrangement enabled us to measure an angular resolution of less than 0.3 mrad below  $\theta_i$  for 8 mrad.

Fig. 3(a) shows a cross-sectional view of the sample. To separate atoms from the substrate a low-density layer that contained source atoms was deposited on a high-density substrate. We used an evaporated Si thin film ( $= 27.0 \text{ nm}$ ) on an Au substrate and a Zn arachidate as a source layer for the fluorescent X-rays.  $z$  was estimated at about 29.8 nm (see §4). The thickness of the Zn arachidate bilayer was 5.5 nm, measured by X-ray diffraction.

### 4. Analysis and discussion

The FXI fringes from a Zn monolayer measured with the IP are shown in Fig. 3(a). These measurements were repeated 30 times for one IP. Each exposure time was 3 s. The output data from the IP reader system were linearly amplified and converted into digital signals. It was easy to treat the output data from the IP; for example, integration along some direction and magnification. The four clear interference fringes were revealed under magnification, as shown in Fig. 3(b).

We used rhodium as the substrate, which can emit fluorescent X-rays of  $L$  radiation ( $\lambda = 0.061$  and  $0.055 \text{ nm}$ ). In this experiment, the fluorescent X-rays from the Rh substrate were not emitted because we tuned the energy level of the polychromatic

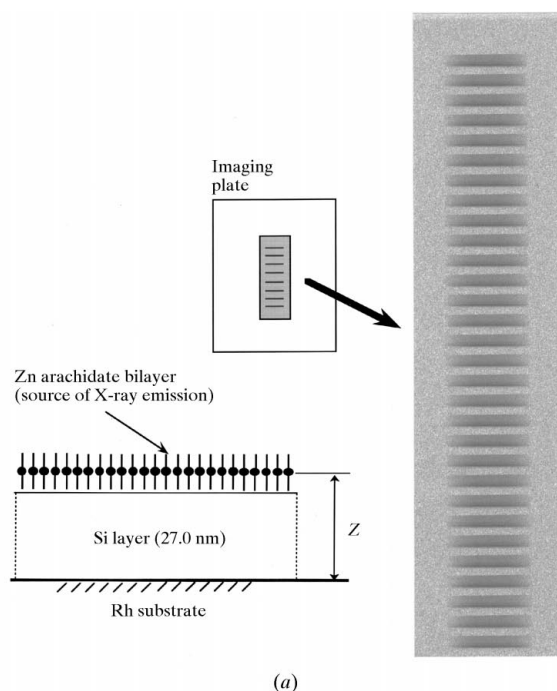
primary X-ray beam without decreasing the intensity of Zn  $K$  radiation. For instance, when we used Au and Pt substrates, which had optically mirrored surfaces as well as the Rh substrate to reflect the fluorescent X-rays (Yanagihara *et al.*, 1992), the Au and Pt substrates emitted fluorescent X-rays of  $L$  radiation ( $\lambda_{\text{Au } L\alpha} = 0.128 \text{ nm}$  and  $\lambda_{\text{Pt } L\alpha} = 0.131 \text{ nm}$ ) very close to that of the  $K$  radiation ( $\lambda_{\text{Zn } K\alpha} = 0.144 \text{ nm}$ ) from Zn atoms. Thus, the fluorescent X-rays from both the Zn monolayer and the Au or Pt substrate were spontaneously emitted with the polychromatic primary beam. In this time-resolved FXI system, we confirmed that it is difficult to observe clear fringes on the IP with substrates of Au and Pt. To monitor the clear FXI patterns with both an IP and a polychromatic primary beam, the sample substrate should offer the following features: (i) a high-density medium and an

optically flat mirror to reflect X-ray radiation; (ii) no X-ray emission from the sample except for the desired fluorescent X-rays.

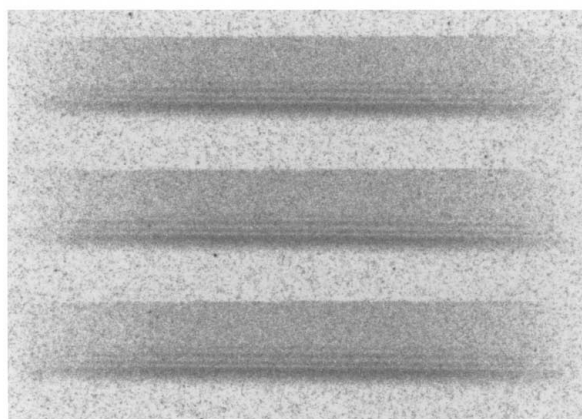
To obtain the exact structural information for the sample, we calculated the theoretical interference fringes by using a  $\chi^2$  minimization fitting to the experimental results measured with a pure-Ge detector. We assumed that a fluorescent X-ray source had a distribution expressed by  $N(z)$ , a Gaussian distribution with a standard deviation ( $2\sigma$ ) of  $\delta z$ , and that it reached a maximum peak at  $z = z_p$ . In the theoretical FXI pattern, we modelled the four homogeneous media, namely air, the LB film containing the monolayer of the Zn arachidate, the evaporated Si thin film and the Rh substrate, as stratified media. From the  $\chi^2$  minimization fitting we obtained a mean Zn position of  $z_p = 29.8 \pm 0.3 \text{ nm}$  and a width of  $\delta z (2\sigma) = 1.4 \pm 0.2 \text{ nm}$ . These values showed 63.8% data accuracy. The FXI pattern from a pure-Ge detector is in close agreement with the theoretical one.

The sum of the FXI pattern along the fringe direction in the IP (Fig. 3b) is shown in Fig. 4. The number of photons per pixel on the IP was calibrated using the observed fluorescent X-ray using a pure-Ge detector with a rectangular slit [ $20 \mu\text{m}$  (V)  $\times$   $12 \text{ mm}$  (H)].

We confirmed that two fluorescent X-rays (Zn  $K\alpha$  and Zn  $K\beta$ ) were emitted from the sample in this experiment. To analyse the FXI patterns from the IP data which consist of the mixed fringes from Zn  $K\alpha$  and Zn  $K\beta$ , we measured the intensity ratio Zn  $K\alpha$ /Zn  $K\beta$  ( $= 5.5$ ) with a pure-Ge detector. We assumed that the IP has approximately the same sensitivity for Zn  $K\alpha$  lines as for Zn  $K\beta$  lines. In the next calculation, we used the optical indices parameters of the above calculation except for those of  $z_p$  and  $\delta z$  ( $2\sigma$ ). Fig. 4 shows the theoretical mixed FXI pattern, which is in close agreement with the observed FXI pattern from the IP. From the  $\chi^2$  minimization fitting, we obtained a mean Zn position of  $z_p = 29.6 \pm 1.0 \text{ nm}$  and a width of  $\delta z (2\sigma) = 4.0 \pm 0.8 \text{ nm}$ . These values show 63.8% data accuracy. The structural information from the IP is in close agreement with the theoretical data. This result shows that we can analyse the monitored FXI pattern from the two-dimensional non-energy-dispersive detector as the mixed FXI pattern of  $K\alpha$  and  $K\beta$  lines.



(a)



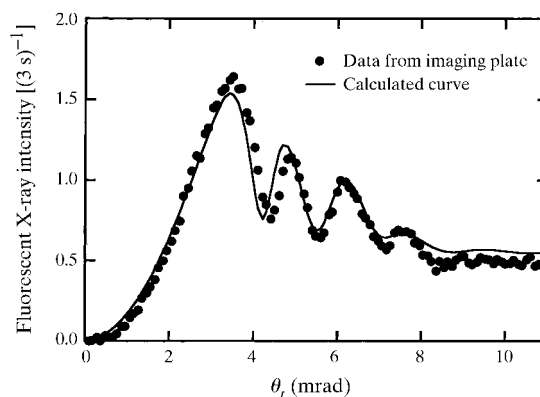
(b)

**Figure 3**

(a) Structure of the sample: cross section of a monolayer of Zn arachidate on the evaporated Si thin film. We used an Rh substrate. The observed interference fringes (right) from the Zn monolayer were measured with the IP. The exposure time was 3 s. (b) The four clear fringes were revealed under magnification. The brighter region corresponds to a higher X-ray intensity.

## 5. Conclusions

We observed fluorescent X-ray interference fringes from the Zn monolayer on the Rh surface with less than 3 s of exposure time.

**Figure 4**

The FXI fringes (closed circles) of the integrated intensity along the fringe direction in Fig. 3(b), and the calculated FXI fringes.

The time-resolved (high-speed) FXI technique comprises the following elements: (i) a polychromatic primary X-ray beam generated from synchrotron radiation; (ii) no X-ray emission from the sample except for the desired fluorescent X-rays under the restricted conditions of X-ray excitation; (iii) high resolution and two-dimensional detector system to integrate along the fringe direction.

The time-resolved FXI technique can be used to observe vertical conformational changes of a biomolecular system, such as molecular recognition between the ligand and the binding protein, the folding processes of protein molecules, and dynamic movement of a membrane. To obtain accurate three-dimensional information about the structure of biomolecules with the time-resolved FXI technique, the arrangement of the biomolecules should be controlled on the substrate surface. Recently, many scientists have succeeded in control-

ling the arrangement of an organic thin film on a substrate surface.

#### References

- Bedzyk, M. J., Bommarito, G. M. & Schildkraut, J. S. (1989). *Phys. Rev. Lett.* **62**, 1376–1379.
- Born, M. & Wolf, E. (1980). *Principles of Optics*, 6th ed. New York: Pergamon.
- Hirai, Y., Waki, I., Hayakawa, K., Kuroishi, K., Yasaka, Y., Kanaya, N., Satow, Y. & Sato, S. (1993). *Nucl. Instrum. Methods*, **A327**, 256–264.
- Miyahara, J., Takahashi, K., Amemiya, Y., Kamiya, N. & Satow, Y. (1986). *Nucl. Instrum. Methods*, **A246**, 572–578.
- Sasaki, Y. C., Suzuki, Y. & Ishibashi, T. (1994). *Science*, **263**, 62–64.
- Sasaki, Y. C., Suzuki, Y., Tomioka, Y. & Fukuhara, A. (1993). *Phys. Rev. B*, **48**, 7724–7726.
- Tegze, M. & Faigel, G. (1996). *Nature (London)*, **380**, 49–51.
- Yanagihara, M., Machara, T., Yamamoto, M. & Namioka, T. (1992). *Proc. SPIE*, **1720**, 246–251.